Journal of Molecular Modeling (2020) 26: 117
https://doi.org/10.1007/s00894-020-04372-x

ORIGINAL PAPER

Theoretical analysis of the regio- and stereoselective synthesis of spiroisoxazolines

Nivedita Acharjee[1]

Received: 17 February 2020 / Accepted: 30 March 2020 / Published online: 7 May 2020

Abstract

The [3+2] cycloaddition (32CA) reaction of benzonitrile oxide to α-methylene cyclopentanone and propionitrile oxide to γ-methyl-α-methylene-γ-butyrolactone, yielding regio- and stereochemically defined spiroisoxazolines, has been studied at the MPWB1K/6-311G(d,p) computational level. These processes proceed by a *one-step* mechanism through asynchronous transition states. *Ortho* regioselectivity and *anti* diastereofacial selectivity are predicted in complete agreement with the experimental outcomes.

Keywords Transition state · Activation energy · Spiroisoxazolines

Introduction

Spiroisoxazolines are a structurally diverse class of biologically active candidates [1–8]. Being an integral part of several natural products, such as calafianin [1, 2], aerothionin [3], agelorins [4] and psammaplysins [5], spiroisoxazolines have received special attention in organic synthesis owing to their wide therapeutic potential. The anticancer properties of the spiroisoxazoline analogues are well documented [6], while in 2017, the spiroisoxazoline SMARt-420 has been identified to revert antibiotic resistance [7], a rapidly increasing health concern. Recently, in 2019, Pratap and coworkers [8] reported the anti-proliferative and antimalarial activities of the spiroisoxazoline derivatives.

The [3+2] cycloaddition (32CA) reactions of nitrile oxides to exocyclic double bonds is the most versatile method for the synthesis of spiroisoxazolines [9]. Numerous studies [6, 9, 10] have been devoted by medicinal chemists to target spiroisoxazoline derivatives from 32CA reactions of nitrile oxides to olefins with exocyclic double bonds. These reactions yield regioisomeric spiroisoxazolines (see Scheme 1) or regio- and stereoisomeric spiroisoxazolines depending on the reagents (see Scheme 2).

Predictability of the regio- and stereochemical outcome of these 32CA reactions depends on the careful examination of the reaction mechanism. Computational studies have come to aid to obtain a precise prediction and analysis of the mechanism, selectivity and reactivity of chemical reactions since the last two decades. Density functional theory [11] has found its place in the characterization of reactants, products, transition state structures (TSs) and intermediates on the potential energy surface (PES) [12] defined under the transition state theory [13]. Since 2000 [14], the location of TSs of several 32CA reactions have been studied in detail, and in 2017, Jasiński and coworkers performed DFT studies to locate the electronic stationary points along the PES of the 32CA reactions of benzonitrile-*N*-oxides and nitroethenes [15]. The MPWBIK functional has been recently stressed [16] in 2018 as a suitable system for the analysis of 32CA reactions. The reaction selectivity and activation parameters of several 32CA reactions have been examined using MPW functional [17, 18] and has provided reasonably good insight of the involved transition states. Herein, nitrile oxide cycloadditions to monosubstituted alkene derivatives with an exocyclic double bond are studied using MPW functional to understand the origin of regio- and diastereofacial selectivity in the synthesis of spiroisoxazolines. Muhlstudt et al. [19] performed nitrile oxide cycloadditions with a wide range of methylene ketones and obtained complete regioselectivity. The 32CA reaction

Electronic supplementary material The online version of this article (https://doi.org/10.1007/s00894-020-04372-x) contains supplementary material, which is available to authorized users.

✉ Nivedita Acharjee
nivchem@gmail.com

[1] Department of Chemistry, Durgapur Government College, Durgapur, Paschim Bardhaman, West Bengal 713214, India

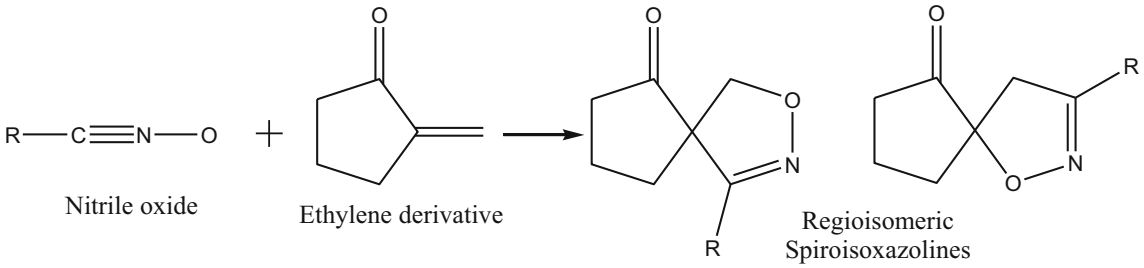

Scheme 1 Synthesis of regioisomeric spiroisoxazolines

of benzonitrile oxide, BNO 1, to α-methylene cyclopentanone, MCP 2, experimentally performed by Muhlstudt et al. [19] (see Scheme 3), has been selected as the first computational model to understand the regioselectivity.

These 32CA reactions of propionitrile oxide with substituted methylene butyrolactones afford regioselective products with 80–100% facial selectivity in favour of the *anti* addition product [20]. The 32CA reaction of propionitrile oxide, PNO 4, to γ-methyl-α-methylene-γ-butyrolactone, MBL 5, experimentally performed by Paul savage et al. [20] (see Scheme 4), has been chosen as the second computational model to understand the facial selectivity in the synthesis of spiroisoxazolines.

Initially, the nature of interactions between the reactants in an elementary cycloaddition step is probed from the analysis of standard global and local reactivity indices. Subsequently, all theoretically possible reaction paths for the 32CAs are examined, and the obtained energetics is analysed.

Computational methods

The Berny analytical gradient optimization method was used [21, 22] with the MPWB1K functional [23] in conjunction with the 6-311G(d,p) basis set [24]. The optimized geometries were then characterized at the same level to ensure that the reactants and products did not have any imaginary frequency and the transition states had one and only one imaginary frequency. The intrinsic reaction coordinate (IRC) [25] pathways of the investigated CAs were traced using the second order Gonzalez-Schlegel integration method [26, 27]. Solvent effects of tetrahydrofuran (THF) and benzene were taken into account using the polarizable continuum model (PCM) [28, 29] in the framework of the self-consistent reaction field (SCRF) [30–32]. Enthalpies, entropies and Gibbs free energies were calculated at reaction conditions 298 K (25 °C) and 1 atm in THF and benzene.

The global reactivity indices, electronic chemical potential μ and chemical hardness η, were calculated from the HOMO (E_{HOMO}) and LUMO (E_{LUMO}) energies using the following equations [33]:

$$\mu \approx (E_{HOMO} + E_{LUMO})/2; \eta \approx E_{LUMO} - E_{HOMO}$$

The electrophilicity index ω is expressed in terms of the electronic chemical potential μ and chemical hardness η by the following equation [33, 34]:

$$\omega = \mu^2/2\eta$$

The relative nucleophilicity index N [35] is expressed as

$$N = E_{HOMO} - E_{HOMO(tetracyanoethylene)}$$

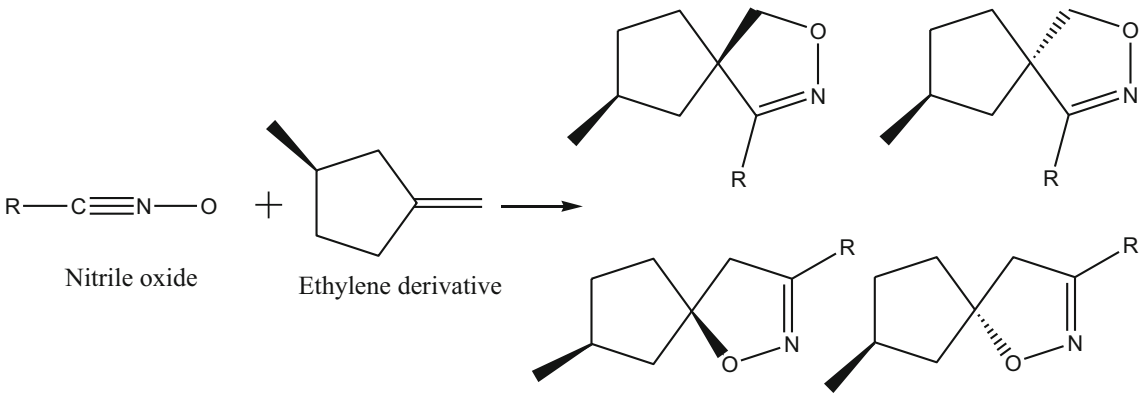

Scheme 2 Synthesis of regio- and stereoisomeric spiroisoxazolines

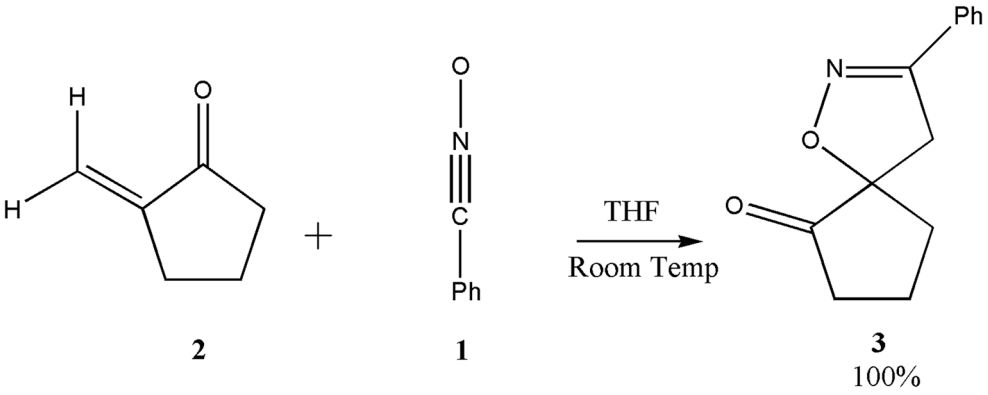

Scheme 3 Regioselective 32CA reaction of benzonitrile oxide, BNO 1, to α-methylene cyclopentanone, MCP 2

The electrophilic P_k^+ and nucleophilic P_k^- Parr functions [36] are calculated using the following equations:

$$P_k^+ = \rho_s^{ra}(r) \text{ (for nucleophilic attack)}$$
$$P_k^- = \rho_s^{rc}(r) \text{ (for electrophilic attack)}$$

where $\rho_s^{ra}(r)$ and $\rho_s^{rc}(r)$ are the Mulliken atomic spin densities of radical anion and radical cation respectively.

All computations were performed using the Gaussian 03 suite of programmes [37]. Topological analysis of the electron localization function (ELF) [38–40] and quantum theory of atoms in molecules (QTAIM) [41] parameters for the reactants and the TSs are also performed. These are collected in the supplementary material.

Analysis of interactions between the reactants

Conceptual density functional theory-based global and local reactivity indices [33] have been used to analyse the interactions between reactants in several biomolecular processes, especially 32CA reactions [see, e.g. 15–18]. A similar approach has also been applied in this study. The calculated global reactivity indices of BNO 1, MCP 2, PNO 4 and MBL 5 are given in Table 1. These indices are calculated at B3LYP/6-31G(d) level since the electrophilicity [34], and nucleophilicity [35] scales are defined in literature at this computational level to characterize reactants in organic reactions.

The electronic chemical potential, μ, of BNO 1, $\mu = -3.81$ eV, is similar to that of MCP 2, $\mu = -4.00$ eV, which indicates a corresponding non-polar character of the 32CA reaction, while PNO 4 shows higher electronic chemical potential, $\mu = -2.91$ eV, relative to MBL 5 with $\mu = -4.22$ eV. This predicts some polar character for the 32CA reaction of PNO 4 to MBL 5.

The electrophilicity ω indexes of BNO 1 and MCP 2 are 1.45 and 1.60 eV, respectively, BNO 1 being classified in the borderline of strong and moderate electrophiles (0.80 eV < ω < 1.50 eV) and MCP 2 being classified as strong electrophile (ω > 1.50 eV) within the electrophilicity scale [34]. PNO 4 with electrophilicity index $\omega = 0.57$ eV is classified as a marginal electrophile while MBL 5 with $\omega = 1.49$ eV as a strong electrophile.

In 2004, Domingo [42] established that the asynchronicity in bond formation is controlled by the electrophilic ethylene derivative irrespective of the polar character of the 32CA reaction. Thus, the most electrophilic centre of the ethylene

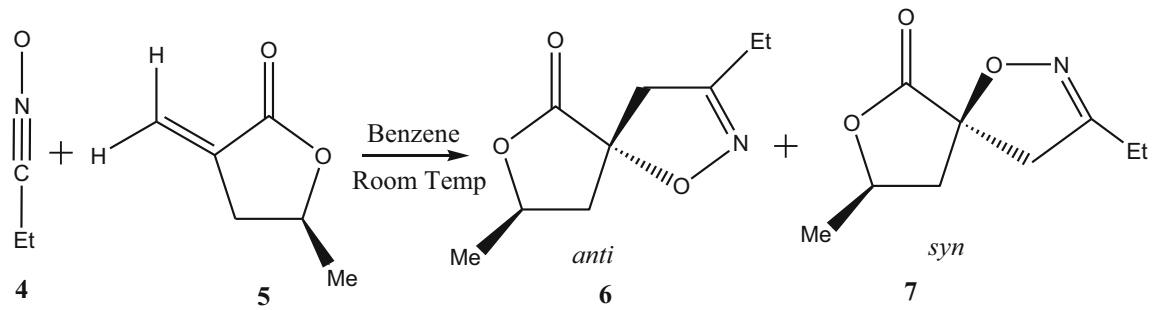

Scheme 4 Stereo- and regioselective 32CA reaction of propionitrile oxide, PNO 4, to γ-methyl-α-methylene-γ-butyrolactone, MBL 5

Table 1 B3LYP/6-31G(d) calculated electronic chemical potential μ, chemical hardness η, global electrophilicity ω and global nucleophilicity N, in eV, of benzonitrile oxide BNO 1, α-methylene cyclopentanone MCP 2, propionitrile oxide PNO 4 and γ-methyl-α-methylene-γ-butyrolactone MBL 5

	μ/eV	η/eV	ω/eV	N/eV
1	− 3.81	5.01	1.45	2.80
2	− 4.00	5.01	1.60	2.61
4	− 2.91	7.46	0.57	2.48
5	− 4.22	5.99	1.49	1.90

The nucleophilicity N index of BNO 1, MCP 2 and PNO 4 is 2.80, 2.61 and 2.48 eV, respectively, being classified as moderate nucleophiles with $N < 3$ eV within the nucleophilicity scale [41], while MBL 5 is classified as a marginal nucleophile with $N < 2$ eV

derivative is always involved in the formation of the first new single bond. Consequently, for 32CA reactions of BNO 1 and PNO 4 to MCP 2 and MBL 5, the electrophilic P_k^+ Parr functions [36] of MCP 2 and MBL 5 were analysed (see Fig. 1). The nucleophilic P_k^- Parr functions of BNO 1 and PNO 4 were also computed. The Mulliken atomic spin densities are given in Fig. 1.

For the C4–C5 bond, the electrophilic P_k^+ Parr functions of C4 and C5 centres in MCP 2, 0.50 and 0.01, respectively, and in MBL 5, 0.58 and 0.09, respectively, indicate that the first single bond will involve the C4 carbon. Finally, the O1 oxygen of BNO 1 and PNO 4 with $P_k^- = 0.45$ and 0.67, respectively, presents the most nucleophilic activation, while the C3 is lesser nucleophilically activated in BNO 1 with $P_k^- = 0.02$ and in PNO 4 with $P_k^- = 0.28$.

Analysis of the energy profile and geometry of transition states

32CA reaction of benzonitrile oxide BNO 1 to α-methylene cyclopentanone MCP 2

Due to the non-symmetry of methylene cyclopentanone MCP 2, two regioisomeric reaction paths, labelled *ortho* and *meta* (see Scheme 5), are feasible for this 32CA reaction. The *ortho* reaction path is associated with the formation of O1–C5 and C3–C4 bonds, while the *meta* channel involves formation of O1–C4 and C3–C5 bonds. Stationary points along these four reaction paths were searched in this study, which allowed locating and characterizing the reagents, BNO 1 and MCP 2, two transition states, i.e. TS1 and TS2, and the corresponding cycloadducts CA1 and CA2 (see Scheme 5). Cycloadduct CA1 is the *ortho* product, and CA2 is the *meta* product. This 32CA reaction follows *one-step* mechanism. The relative energies, enthalpies and free energies of products and TSs in gas phase as well as THF are given in Table 2.

Analysis of the relative energies leads to some appealing conclusions. The activation energies are 11.4 kcal mol^{-1} (TS1) and 15.9 kcal mol^{-1} (TS2) in gas phase and 13.4 kcal mol^{-1} (TS1) and 18.1 kcal mol^{-1} (TS2) in THF, with the 32CA reaction being strongly exothermic with 48.3 kcal mol^{-1} (CA1) and 43.4 kcal mol^{-1} (CA2) in gas phase and 46.4 kcal mol^{-1} (CA1) and 41.6 kcal mol^{-1} (CA2) in THF (see Table 2). The inclusion of THF increases the activation enthalpies by 2.3 kcal mol^{-1} (TS1) and 2.6 kcal mol^{-1}(TS2) as a consequence of a larger solvation of the reagents than TSs [43]. The activation energy 11.4 kcal mol^{-1} associated with

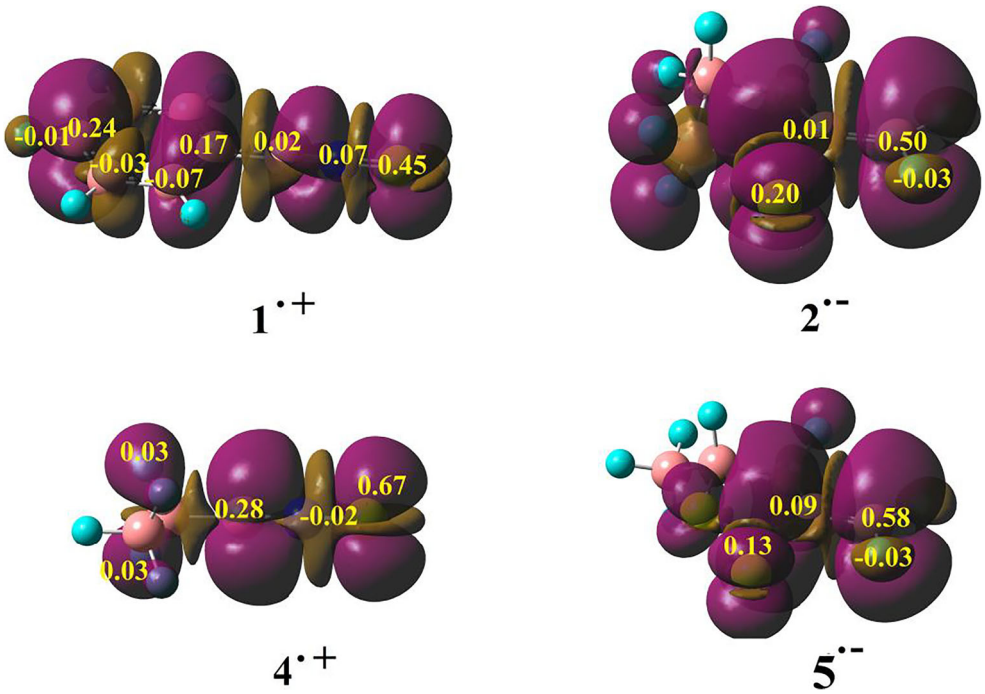

Fig. 1 Three-dimensional representation of the Mulliken atomic spin densities (isovalue = 0.0004) of radical anions 2^- and 5^- and radical cations 1^+ and 4^+ together with the electrophilic P_k^+ Parr functions of MCP 2 and MBL 5 and the nucleophilic P_k^- Parr functions of BNO 1 and PNO 4. Purple regions correspond to positive values, while the brown regions correspond to negative regions of the Mulliken atomic spin densities

Scheme 5 Studied reaction paths of the 32CA reaction of BNO 1 to MCP 2

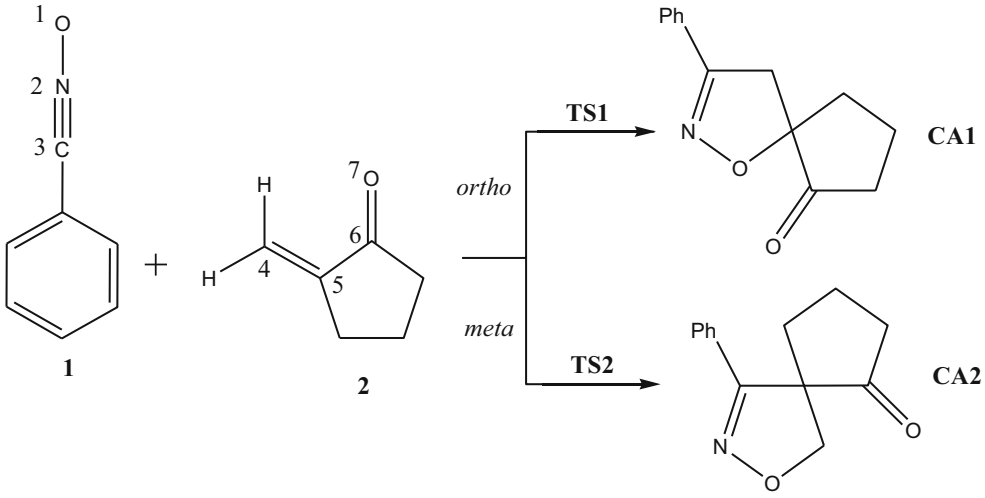

TS1 is lower than that associated with the non-polar 32CA reaction of BNO 1 with methyl acrylate, 12.3 kcal mol^{-1}, in which the *ortho* TS is lower than *meta* TS by only 1.6 kcal mol^{-1} [44]. For the 32CA reaction of BNO 1 and MCP 2, the most favourable reaction path is associated with the *ortho* approach mode, yielding the cycloadduct CA1 via TS1 in complete agreement with the experimental results [19]. This 32CA reaction is completely regioselective, as TS1 is 4.5 kcal mol^{-1} lower in activation energy than TS2 in gas phase and by 4.7 kcal mol^{-1} in THF. The formation of product CA1 is strongly exothermic which makes the reaction irreversible.

Table 2 MPWB1K/6-311G(d,p) calculated ΔE, ΔH and ΔG in kcal/mol of products and transition states for the 32CA reactions

Entry	TS/CA	Medium	ΔE (kcal/mol)	ΔH (kcal/mol)	ΔG (kcal/mol)
1	TS1	Gas phase	11.4	11.8	25.0
2	CA1	Gas phase	−48.3	−45.7	−31.4
3	TS2	Gas phase	15.9	16.5	30.8
4	CA2	Gas phase	−43.4	−40.4	−25.3
5	TS1	THF	13.4	14.1	27.3
6	CA1	THF	−46.4	−43.3	−29.2
7	TS2	THF	18.1	19.1	33.4
8	CA2	THF	−41.6	−38.2	−23.2
9	TS3	Gas phase	11.4	11.7	24.7
10	CA3	Gas phase	−48.3	−45.7	−31.0
11	TS4	Gas phase	12.5	12.9	26.1
12	CA4	Gas phase	−45.8	−43.3	−28.9
13	TS5	Gas phase	15.6	16.0	30.1
14	CA5	Gas phase	−44.2	−41.2	−26.2
15	TS6	Gas phase	15.8	16.1	29.4
16	CA6	Gas phase	−45.4	−42.4	−27.6
17	TS3	Benzene	12.6	13.0	25.9
18	CA3	Benzene	−46.6	−44.0	−29.3
19	TS4	Benzene	13.8	14.2	27.3
20	CA4	Benzene	−44.8	−42.2	−27.8
21	TS5	Benzene	17.7	18.2	32.3
22	CA5	Benzene	−42.5	−39.4	−24.5
23	TS6	Benzene	17.6	18.1	31.4
24	CA6	Benzene	−43.8	−40.7	−26.0

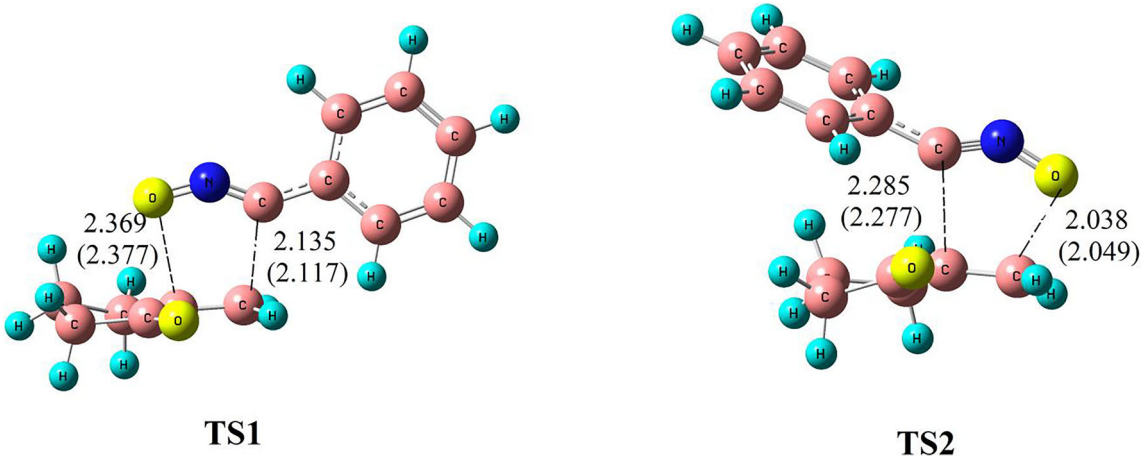

Fig. 2 MPWB1K/6-311G(d,p) optimized transition states for 32CA reaction of BNO 1 and MCP 2. Bond lengths are given in angstrom units. Values in parenthesis indicate the bond lengths calculated in THF

Thermal corrections to the electronic energies give the relative enthalpies in gas phase and THF. The activation enthalpies increase by 0.4 and 0.6 kcal mol^{-1} in gas phase and 0.7 and 1.0 kcal mol^{-1} in THF relative to the activation energies, while reaction enthalpies decrease by 2.6 and 3.0 kcal mol^{-1} in gas phase and 3.1 and 3.4 kcal mol^{-1} in THF relative to the reaction energies. Inclusion of the entropies to enthalpies strongly increases the activation Gibbs energies by 13.2 and 14.3 kcal mol^{-1} in gas phase and THF, while the reaction Gibbs energies show a sharp decrease by 14.3 and 15.1 kcal mol^{-1} in gas phase and 14.1 and 15.0 kcal mol^{-1} in THF.

The activation Gibbs free energy of cycloadduct CA1 becomes 25.0 kcal mol^{-1} in gas phase and 27.3 kcal mol^{-1} in THF, the 32CA reaction being strongly exergonic by

Scheme 6 Studied reaction paths of the 32CA reaction of propionitrile oxide PNO 4 to γ-methyl-α-methylene-γ-butyrolactone MBL 5

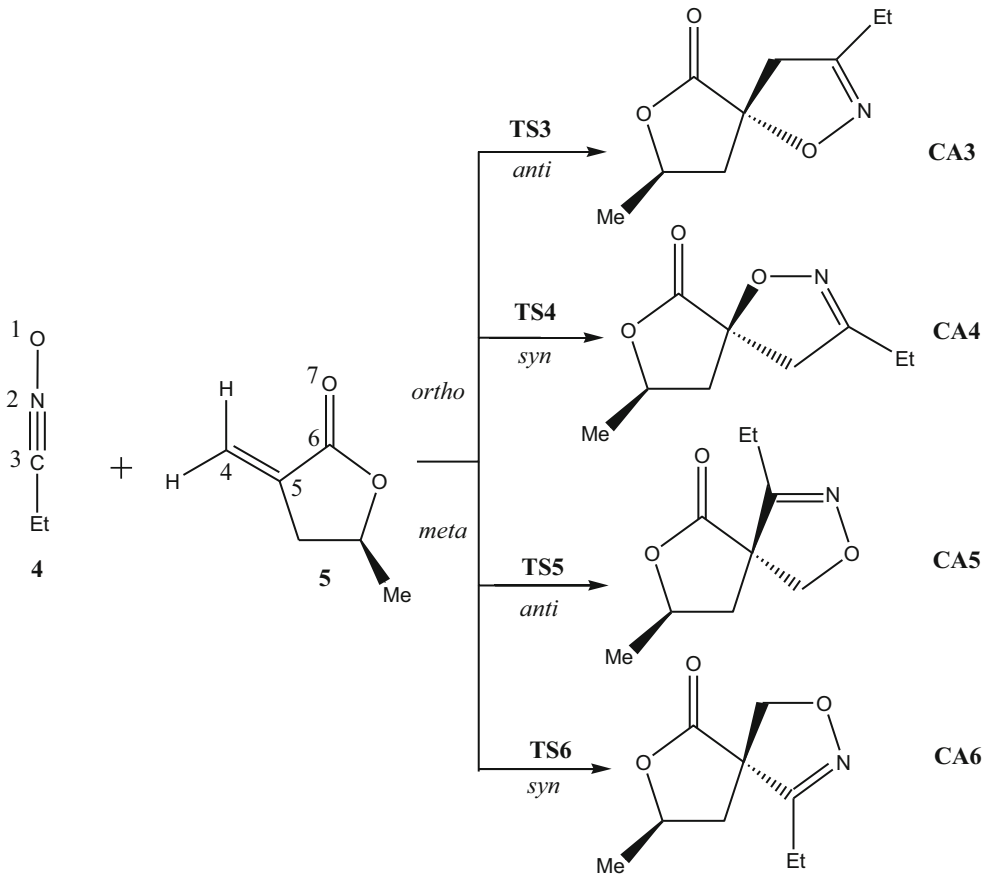

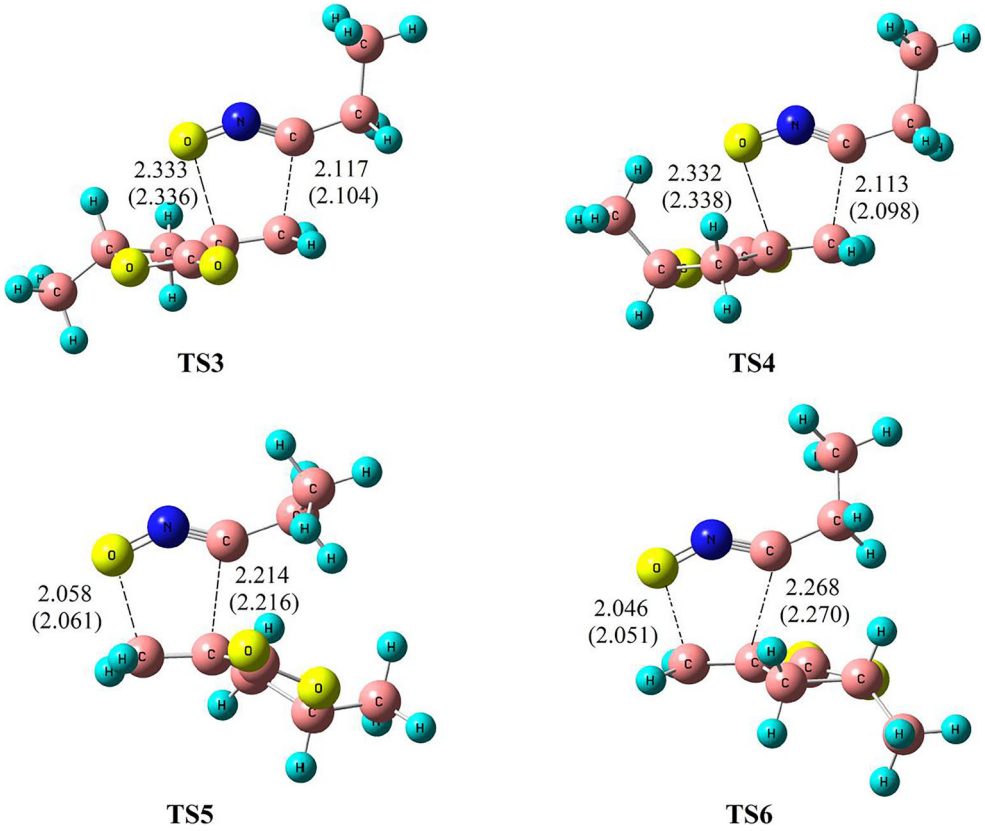

Fig. 3 MPWB1K/6-311G(d,p) optimized transition states for 32CA reaction of PNO 4 and MBL 5. Bond lengths are given in angstrom units. Values in parenthesis indicate the bond lengths calculated in benzene

31.4 kcal mol^{-1} in gas phase and 29.2 kcal mol^{-1} in THF. Figure 2 shows the optimized geometries of the TSs.

Now, formation of C–C and C–O single covalent bonds begin at a distance of 2.0–1.9 Å and 1.7–1.6 Å [17] respectively, which indicates that the formation of new C–C and C–O covalent bonds has not started in the TSs with C–C and C–O forming bond distances greater than 2.0 Å (see Fig. 2). The forming C–C bond length is shorter than C–O forming bond length at TS1, while the shorter bond length corresponds to the formation of C–O forming bond at TS2. These two TSs show almost similar asynchronicity, and inclusion of the solvent effects of THF slightly changes the forming bond lengths at these two TSs.

32CA reaction of propionitrile oxide PNO 4 to γ-methyl-α-methylene-γ-butyrolactone MBL 5

Due to the non-symmetry of both the reagents PNO 4 and MBL 5, different stereo- and regioisomeric paths exist for this 32CA reaction. The two regioisomeric reaction paths labelled *ortho* and *meta* and the two diastereofacial isomeric reaction paths, labelled *syn* and *anti*, associated with the participation of nitrile oxide and exocyclic double bond addition have been considered here (see Scheme 6). The *ortho* regioisomeric channel is associated with the formation of C3–C4 and C5–O1 bonds, while the *meta* path involves formation of C3–C5 and C4–O1 bonds. The *anti* diastereofacial reaction path is associated with the addition opposite to the methyl substituent, while the *syn* diastereofacial reaction path is associated with the addition to the same face of the methyl substituent as coined by Savage and coworkers [20] for this 32CA reaction.

Along these four reaction paths, four TSs, i.e. TS3, TS4, TS5 and TS6, were located and characterized and the corresponding cycloadducts, i.e. CA3, CA4, CA5 and CA6. This 32CA reaction follows a *one-step* mechanism, and the relative energies in gas phase and benzene are given in Table 2. The activation energies range from 11.4 (TS3) to 15.8 (TS6) kcal mol^{-1} in gas phase and from 12.6 (TS3) to 17.7 (TS5) kcal mol^{-1} in benzene, with this 32CA reaction being strongly exothermic from −44.2 (CA5) to −48.3 (CA3) kcal mol^{-1} in gas phase and −42.5 (CA5) to −46.6 (CA3) kcal mol^{-1} in benzene. Inclusion of solvent effects in benzene increases the activation enthalpy by 1.3–2.2 kcal mol^{-1} as a consequence of a larger solvation of the reagents than TSs [44]. This 32CA reaction is completely *ortho* regioselective, as TS5 and TS6 are higher in energy than TS3 by 4.2 and 4.4 kcal mol^{-1} in gas phase and 5.1 and 5.0 kcal mol^{-1} in benzene. The activation energy of TS4 is higher in energy than TS3 by 1.1 kcal mol^{-1} in gas phase and by 1.2 kcal mol^{-1} in benzene, which accounts for the 81:19 diastereomeric ratio of *ortho/anti* and *ortho/syn* products obtained experimentally in benzene at room temperature [20].

The inclusion of thermal corrections to the electronic energies causes minimal increase in activation enthalpies by 0.3–0.5 kcal mol^{-1}, while the reaction enthalpies are increased by 2.5–3.1 kcal mol^{-1}. The activation Gibbs free energies are increased by between 12.9 and 14.1 kcal mol^{-1} relative to the activation enthalpies, while the reaction Gibbs energies are strongly increased by between 14.4 and 15.0 kcal mol^{-1}, which is due to the unfavourable entropies associated with this 32CA process. The relative Gibbs free energies clearly account for the complete *ortho* regioselectivity and *anti* diastereofacial selectivity experimentally observed [20].

The optimized geometries of four TSs are given in Fig. 3.

At the *ortho* TSs, TS3 and TS4, the length of forming C5–O1 bond is greater than that of the forming C3–C4 bond, while at the *meta* TSs, TS5 and TS6, the length of forming C3–C5 bond is greater than that of the forming C4–O1 bond. Forming C3–C4 and C5–O1 bond distances greater than 2.0 Å indicates that no covalent bond formation has begun yet in any of the four TSs. *Meta* and *ortho* TSs show almost similar asynchronicity. Inclusion of solvent effects in benzene scarcely changes the forming bond lengths.

Conclusions

The 32CA reactions of α-methylene cyclopentanone and γ-methyl-α-methylene-γ-butyrolactone to benzonitrile oxide and propionitrile oxide, yielding spiroisoxazolines with regio- and stereoselective control, have been studied at MPWB1K/6-311G(d,p) level of theory. Analysis of Parr functions indicates the initiation from the unsubstituted carbon atom of the ethylene derivative. These 32CA reactions present activation enthalpy of 11.8 and 11.7 kcal mol^{-1} in gas phase, while 14.1 and 12.9 kcal mol^{-1} are the respective calculated values in THF and benzene. Analysis of the activation Gibbs free energies indicates that these 32CA reactions are completely *ortho* regioselective and the second reaction proceeds through *anti* diastereofacial selectivity under kinetic control, in complete agreement with the experimental findings.

Acknowledgments The author is thankful to Professor Manas Banerjee, Retired Professor, at The University of Burdwan, India, for his kind cooperation. The author also acknowledges the help and support of Professor Luis R Domingo, Professor, at the University of Valencia, Spain, for important clarifications in several studies related to the concept of 32CA reactions.

References

1. Encarnacion RD, Sandoval E, Malmstrom J, Christophersen C (2000) Calafianin, a bromotyrosine derivative from the marine sponge Aplysina gerardogreeni. J Nat Prod 63:874–875. https://doi.org/10.1021/np990489d
2. Bardhan S, Schmitt DC, Porco JA (2006) Total synthesis and stereochemical assignment of spiroisoxazoline natural product (+) calafianin. Org Lett 8:927–930. https://doi.org/10.1021/ol053115m
3. Ogamino T, Obata R, Nishiyama S (2006) Asymmetric synthesis of aerothionin, a marine dimeric spiroisoxazoline natural product, employing optically active spiroisoxazoline derivative. Tetrahedron Lett 47:727–730. https://doi.org/10.1016/j.tetlet.2005.11.097
4. Konig GM, Wright AD (1993) Agelorins A and B, and 11-epi-fistularin-3,three new antibacterial fistularin-3 derivatives from the tropical marine sponge Agelas oroides. Heterocycles 36:1351–1358. https://doi.org/10.3987/COM-92-6317
5. Perron F, Albizati KF (1989) Chemistry of spiroketals. Chem Rev 89:1617–1661. https://doi.org/10.1021/cr00097a015
6. Khazir J, Singh PP, Reddy M, Hyder I, Shafi S, Sawant SD, Chashoo G, Mahajan A, Alam MS, Saxena AK, Arvinda S, Gupta BD, Sampath Kumar HM (2013) Synthesis and anticancer activity of novel spiro-isoxazoline and spiro-isoxazolidine derivatives of α-santonin. Eur J Med Chem 63:279–289. https://doi.org/10.1016/j.ejmech.2013.01.003
7. Blondiaux N, Moune M, Desroses M, Frita R, Flipo M, Mathys V, Soetaert K, Kiass M, Delorme V, Djaout K, Trebosc V, Kemmer C, Wintjens R, Wohlkönig A, Antoine R, Huot L, Hot D, Coscolla M, Feldmann J, Gagneux S, Locht C, Brodin P, Gitzinger M, Déprez B, Willand N, Baulard AR (2017) Reversion of antibiotic resistance in mycobacterium tuberculosis by spiroisoxazoline SMARt-420. Science 335:1206–1211. https://doi.org/10.1126/science.aag1006
8. Pratap S, Naaz F, Reddy S, Jha KK, Sharma K, Sahal D, Akhter M, Nayakanti D, Kumar HMS, Vandana PK, Shafi S (2019) Anti-proliferative and anti-malarial activities of spiroisoxazoline analogues of artemisinin. Arch Pharm 352:1800192. https://doi.org/10.1002/ardp.201800192
9. Savage GP (2010) Spiro isoxazolines via nitrile oxide 1,3-dipolar cycloaddition reactions. Curr Org Chem 14:1478–1499. https://doi.org/10.2174/138527210791616812
10. Zaki M, Oukhrib A, Akssira M, Berteina-Raboin S (2017) Synthesis of novel spiro-isoxazoline and spiro-isoxazolidine derivatives of tomentosin. RSC Adv 7:6523–6529. https://doi.org/10.1039/C6RA25869G
11. Parr RG, Yang W (1989) Density-functional theory of atoms and molecules, vol 4. Oxford University Press, Oxford, pp 70–86
12. Moss SJ, Coady CJ (1983) Potential-energy surfaces and transition state theory. J Chem Educ 60:455–461. https://doi.org/10.1021/ed060p455
13. Trautz M (1916) Das gesetz der reaktionsgeschwindigkeit und der gleichgewichte in gasen. Bestätigung der additivität von Cv-3/2R. Neue bestimmung der integrationskonstanten und der molekürdurchmesser. Z Anorg Allg Chem 96:1–28
14. Carda M, Portolés R, Murga J, Uriel S, Marco JA, Domingo LR, Zaragozá RJ, Röper H (2010) Stereoselective 1,3-dipolar cycloadditions of a chiral nitrone derived from erythrulose. An experimental and DFT theoretical study. J Org Chem 65:7000–7009. https://doi.org/10.1021/jo0009651
15. Jasiński R, Jasińska E, Dresler E (2017) A DFT computational study of the molecular mechanism of [3 + 2] cycloaddition reactions between nitroethene and benzonitrile N-oxides. J Mol Model 23:13. https://doi.org/10.1007/s00894-016-3185-8
16. Domingo LR, Ríos-Gutiérrez M, Pérez P (2018) A molecular electron density theory study of the reactivity and selectivities in [3+2] cycloaddition reactions of C,N-dialkyl nitrones with ethylene derivatives. J Org Chem 83:2182–2197. https://doi.org/10.1021/acs.joc.7b03093
17. Ríos-Gutiérrez M, Domingo LR (2019) Unravelling the mysteries of the [3+2] cycloaddition reactions. Eur J Org Chem:267–282. https://doi.org/10.1002/ejoc.201800916

18. Domingo LR, Acharjee N (2018) [3+2] Cycloaddition reaction of C-phenyl-N-methyl nitrone to acyclic-olefin-bearing electron-donating substituent: a molecular electron density theory study. ChemistrySelect 3:8373–8380. https://doi.org/10.1002/slct.201801528
19. Muller G, Frischleder H, Muhlstadt M (1969) Mono- und bicyclische _- methylenketone als dipolarophile. J Prakt Chem 311:118–129. https://doi.org/10.1002/prac.19693110117
20. Pereira SM, Savage GP, Simpson GW, Greenwood RJ, Mackay MF (1993) Diastereoselective propionitrile oxide cycloaddition reactions with some γ-substituted α-methylene-γ-butyrolactones. Aust J Chem 46:1401–1412. https://doi.org/10.1071/CH9931401
21. Schlegel HB (1982) Optimization of equilibrium geometries and transition structures. J Comput Chem 3:214–218. https://doi.org/10.1002/jcc.540030212
22. Schlegel HB (1994) Modern electronic structure theory. World Scientific Publishing, Singapore
23. Zhao Y, Truhlar DG (2004) Hybrid meta density functional theory methods for thermochemistry, thermochemical kinetics, and noncovalent interactions: the MPW1B95 and MPWB1K models and comparative assessments for hydrogen bonding and van der Waals interactions. J Phys Chem A 108:6908–6918. https://doi.org/10.1021/jp048147q
24. Hehre WJ, Radom L, Schleyer PVR, Pople JA (1996) Ab initio molecular orbital theory. Wiley, New York. https://doi.org/10.1002/jcc.540070314
25. Fukui K (1970) Formulation of the reaction coordinate. J Phys Chem 74:4161–4163. https://doi.org/10.1021/j100717a029
26. González C, Schlegel HB (1990) Reaction path following in mass-weighted internal coordinates. J Phys Chem 94:5523–5527. https://doi.org/10.1021/j100377a021
27. González C, Schlegel HB (1991) Improved algorithms for reaction path following: higher-order implicit algorithms. J Chem Phys 95:5853–5860. https://doi.org/10.1063/1.461606
28. Tomasi J, Persico M (1994) Molecular interactions in solution: an overview of methods based on continuous distributions of the solvent. Chem Rev 94:2027–2094. https://doi.org/10.1021/cr00031a013
29. Simkin BY, Sheikhet II (1995) Quantum chemical and statistical theory of solutions: a computational approach. Ellis Horwood, London
30. Cossi M, Barone V, Cammi R, Tomasi J (1996) Ab initio study of solvated molecules: a new implementation of the polarizable continuum model. Chem Phys Lett 255:327–335. https://doi.org/10.1016/0009-2614(96)00349-1
31. Cances E, Mennucci B, Tomasi J (1997) A new integral equation formalism for the polarizable continuum model: theoretical background and applications to isotropic and anisotropic dielectrics. J Chem Phys 107:3032–3041. https://doi.org/10.1063/1.474659
32. Barone V, Cossi M, Tomasi J (1998) Geometry optimization of molecular structures in solution by the polarizable continuum model. J Comput Chem 19:404–417. https://doi.org/10.1002/(SICI)1096-987X(199803)19:4<404::AID-JCC3>3.0.CO;2-W
33. Domingo LR, Ríos-Gutiérrez M, Pérez P (2016) Applications of the conceptual density functional theory indices to organic chemistry reactivity. Molecules 21:748 (22 pages). https://doi.org/10.3390/molecules21060748
34. Domingo LR, Aurell MJ, Pérez P, Contreras R (2002) Quantitative characterization of the global electrophilicity power of common diene/dienophile pairs in Diels-Alder reactions. Tetrahedron 58:4417–4423. https://doi.org/10.1016/S0040-4020(02)00410-6
35. Domingo LR, Pérez P (2011) The nucleophilicity N index in organic chemistry. Org. Biomol Chem 9:7168–7175. https://doi.org/10.1039/C1OB05856H
36. Domingo LR, Pérez P, Sáez JA (2013) Understanding the local reactivity in polar organic reactions through electrophilic and nucleophilic Parr functions. RSC Adv 3:1486–1494. https://doi.org/10.1039/C2RA22886F
37. Frisch MJ, Trucks GW, Schlegel HB, Scuseria GE, Robb MA, Cheeseman JR, Montgomery JA Jr, Vreven T, Kudin KN, Burant JC, Millam JM, Iyengar SS, Tomasi J, Barone V, Mennucci B, Cossi M, Scalmani G, Rega N, Petersson GA, Nakatsuji H, Hada M, Ehara M, Toyota K, Fukuda R, Hasegawa J, Ishida M, Nakajima T, Honda Y, Kitao O, Nakai H, Klene M, Li X, Knox JE, Hratchian HP, Cross JB, Bakken V, Adamo C, Jaramillo J, Gomperts R, Stratmann RE, Yazyev O, Austin AJ, Cammi R, Pomelli C, Ochterski JW, Ayala PY, Morokuma K, Voth GA, Salvador P, Dannenberg JJ, Zakrzewski VG, Dapprich S, Daniels AD, Strain MC, Farkas O, Malick DK, Rabuck AD, Raghavachari K, Foresman JB, Ortiz JV, Cui Q, Baboul AG, Clifford S, Cioslowski J, Stefanov BB, Liu G, Liashenko A, Piskorz P, Komaromi I, Martin RL, Fox DJ, Keith T, Al-Laham MA, Peng CY, Nanayakkara A, Challacombe M, Gill PMW, Johnson B, Chen W, Wong MW, Gonzalez C, Pople JA (2004) Gaussian 03, Revision D.01. Gaussian, Inc., Wallingford CT
38. Becke AD, Edgecombe KE (1990) A simple measure of electron localization in atomic and molecular systems. J Chem Phys 92:5397–5403. https://doi.org/10.1063/1.458517
39. Silvi B, Savin A (1994) Classification of chemical bonds based on topological analysis of electron localization functions. Nature 371:686–686. https://doi.org/10.1038/371683a0
40. Yepes D, Murray JS, Pérez P, Domingo LR, Politzer P, Jaque P (2014) Complementarity of reaction force and electron localization function analyses of asynchronicity in bond formation in Diels–Alder reactions. Phys Chem Chem Phys 16:6726–6734. https://doi.org/10.1039/C3CP54766C
41. Bader RFW (1990) Atoms in molecules: a quantum theory. Clarendon Press, Oxford
42. Aurell MJ, Domingo LR, Pérez P, Contreras R (2004) A theoretical study on the regioselectivity of 1,3-dipolar cycloadditions using DFT-based reactivity indexes. Tetrahedron 60:11503–11509. https://doi.org/10.1016/j.tet.2004.09.057
43. Benchouk W, Mekelleche SM, Silvi B, Aurell MJ, Domingo LR (2011) Understanding the kinetic solvent effects on the 1,3-dipolar cycloaddition of benzonitrile N-oxide: a DFT study. J Phys Org Chem 24:611–618. https://doi.org/10.1002/poc.1858
44. Ndassa IM, Adjieufack AI, Ketcha JM, Berski S, Ríos-Gutiérrez M, Domingo LR (2017) Understanding the reactivity and regioselectivity of [3+2] cycloaddition reactions between substituted nitrile oxides and methyl acrylate. A molecular electron density theory study. Int J Quantum Chem 117:e25451. https://doi.org/10.1002/qua.25451